Ab Initio Study of the Role of Entropy in the Kinetics of Acetylene Production in Filament-Assisted Diamond Growth Environments

Yanxin Li* and Donald W. Brenner†

Department of Materials Science and Engineering, North Carolina State University, Raleigh, North Carolina 27695-7907

Xialan Dong‡

Department of Physics, East Carolina University, Greenville, North Carolina 27858

Chiachung Sun

Institute of Theoretical Chemistry, Jilin University, Changchun 130023, P.R. China

Received: August 30, 2005

We present a new theoretical strategy, ab initio rate constants plus integration of rate equations, that is used to characterize the role of entropy in driving high-temperature/low-pressure hydrocarbon chemical kinetics typical of filament-assisted diamond growth environments. Twelve elementary processes were analyzed that produce a viable pathway for converting methane in a feed gas to acetylene. These calculations clearly relate the kinetics of this conversion to the properties of individual species, demonstrating that (1) loss of translational entropy restricts addition of hydrogen (and other radical species) to unsaturated carbon−carbon bonds, (2) rotational entropy determines the direction of the rate-limiting abstraction reactions, and (3) the overall pathway is enhanced by high β-scission reaction rates driven by translational entropy. These results suggest that the proposed strategy is likely applicable to understand gas-phase chemistry occurring in the systems of combustion and other chemical vapor depositions.

I. Introduction

Ab initio theory has progressed to the stage that very accurate data can be generated for a wide range of gas-phase and solid-state processes and structures.[1] Moreover, the results of ab initio calculations often give new and sometimes surprising insights that cannot be obtained from experiment alone. For example, a recent ab initio analysis of the gas-phase environment associated with AlN sublimation growth suggested that the nitrogen-containing growth species was not N_2 as had been assumed, but rather Al_mN clusters of $m = 2, 3, 4$.[2]

In this paper, we revisit an important process in the filament-assisted chemical vapor deposition (FACVD) of diamond films,[3−8] the creation of acetylene from methane under growth conditions,[7] using ab initio methods. Our intent is not to recalculate species concentrations—a number of kinetic calculations have been performed[8−22]—but rather to use ab initio methods to understand in new detail the competing roles of entropy and enthalpy in driving this chemistry. In this respect C_2H_2 production from CH_4 is an excellent system in which to apply ab initio methods for understanding chemical dynamics because while there are accurate experimental data to which the calculations can be validated, a detailed analysis of the basis for the kinetic competition among these rates in terms of fundamental properties of the reactiving species has not been previously attempted.

In FACVD, a hydrocarbon feed gas, typically with a H_2/CH_4 ratio by volume higher than 99%, flows over a hot filament. The filament creates supersaturated atomic hydrogen, which in turn leads to reactive species containing radicals and unsaturated C−C bonds in the feed gas. The atomic hydrogen also creates reactive sites on the substrate via hydrogen abstraction and may help etch non-diamond carbon co-deposited on the substrate. The gas-phase chemistry associated with FACVD has been characterized theoretically using both thermodynamic[9−13] and kinetic[8,14−18] models, as well as simulations that include detailed transport effects within reaction chambers.[19−22] These studies have attempted to explain the presence of various species typically observed in reaction chambers, as well as to reproduce various experimental trends such as the effects of atomic hydrogen, temperature, pressure, and initial methane concentration on diamond growth. Goodwin and Butler, for example, suggested that the abundance of acetylene observed experimentally in FACVD growth chambers can be accounted for by noting that although the reaction $2CH_4 \rightarrow C_2H_2 + 3H_2$ is endothermic at the high temperatures and low pressures typical of FACVD, it has a negative Gibbs free energy due mainly to an increase in translational entropy.[7]

* Corresponding author. Phone: (919)889-8294. Fax: (919)515-7724. E-mail address: yanxinl@hotmail.com.

† E-mail address: brenner@eos.ncsu.edu.

‡ Formerly with the Department of Chemistry, Jilin University. E-mail address: xd0801@mail.ecu.edu.

10.1021/jp054914p CCC: $33.50
Published on Web 12/08/2005

Using ab initio data in conjunction with transition state theory (TST)[23] has two main advantages relative to previous studies of FACVD chemistry. First, it explicitly separates contributions to reaction rates from various entropy and enthalpy sources, allowing their effects on the reaction kinetics to be delineated. With the use of experimental rate constants alone, it is not possible to obtain this new and detailed insight because multiple physical quantities cannot be unequivocally decomposed from a few parameters of the Arrhenius formula. Second, this approach produces a comprehensive set of rates with a consistent level of accuracy for all relevant reactions and temperatures, paving a proper way to attribute the complex kinetics to single species properties. Therefore ab initio TST analysis uniquely leads to important new insights into the kinetic driving forces largely responsible for gas-phase chemical kinetics at high temperatures and low pressures. We believe that the theoretical strategy used in this paper is also applicable to understand gas-phase chemistry occurring in the systems of combustion and other chemical vapor depositions.

The paper is organized as follows. In the next section, a set of six elementary reactions with 12 rates (a backward and forward rate for each reaction) is established based on typical FACVD conditions that provide a viable pathway for converting between methane and acetylene. The reactions include unimolecular dissociation and bimolecular hydrogen−hydrocarbon molecule collisions, and the analysis includes consideration of collision effects. Presented in section III are calculation details regarding ab initio structures of species and their transition states, TST rate constants,[23] and the integration of rate equations. The results of the calculations are given in section IV. The results include total energies, vibrational frequencies, electronic energies, and rotational inertia for all relevant molecules and transition states. The calculated rates as a function of temperature are given together with experimental rates for validation. The kinetics of methane conversion to acetylene is presented based on rate constant analysis. In the kinetics of this reaction, the rate-limiting step is hydrogen abstraction and the irreversibility of the overall pathway is enhanced by high β-scission reaction rates. The integration of rate equations over the viable pathway is performed, demonstrating the consistency between experimental measurements and the proposed kinetics. Decomposition of the proposed kinetics into single species properties appears in section V, along with a discussion of specific entropy effects on the various rates and implications for understanding FACVD gas-phase chemical kinetics. Specifically, it is shown that H_2 rotational entropy determines the direction of hydrogen abstraction reactions and that the creation of translational degrees of freedom causes high β-scission reaction rates. Hydrogen atom addition to unsaturated carbon−carbon bonds is limited by the loss of translational entropy that overwhelms those energy contributions to the free energy caused by σ-bond making and π-bond breaking.

II. Reaction Model

To investigate the kinetics of diamond film FACVD, a viable set of elementary processes is needed on which an analysis can be carried out. Typical gas-phase conditions in FACVD reactors consist of high temperatures (1100−2300 K), low pressures (20−50 Torr), slow flow rates (100 standard cubic centimeters per minute (sccm)), and a high H_2 mole fraction (>99%). Under these conditions, collision frequencies for trimolecular and higher order reactions are small; therefore only unimolecular and bimolecular reactions are considered. The unimolecular reactions considered consist of β-scission reactions[24] of the form $\{C_2H_x \rightarrow C_2H_{x-1} + H,\ x = 3,5\}$. In these reactions, a C−H bond β to a radical is broken, allowing formation of a C−C double or triple bond. Unimolecular reactions involving C_3 radicals are ignored because they are not typically observed in the gas phase under growth conditions. Single carbon bi- and triradicals are also ignored due to their instability relative to C_2H_x uniradicals.

Candidate bimolecular reactions can be conveniently divided into three types, reactions between two radicals, reactions between two molecules, and reactions between a radical and a molecule. Radical−radical reactions are ignored (with one exception, see below) because they are expected to proceed quickly and therefore are not rate-limiting. Molecule−molecule reactions are also ignored because these reactions are likely too slow to significantly contribute to the gas-phase kinetics. Of the radical−molecule reactions remaining, those involving two hydrocarbon species are ignored due to the low collision probabilities resulting from the small hydrocarbon concentrations. This leaves reactions in which a hydrogen atom (the radical) abstracts hydrogen from a hydrocarbon molecule, its reverse reaction in which a hydrocarbon radical abstracts hydrogen from H_2, and hydrogen atom addition to π-bond containing hydrocarbons.

This analysis yields the following set of elementary reactions and relevant transition states:

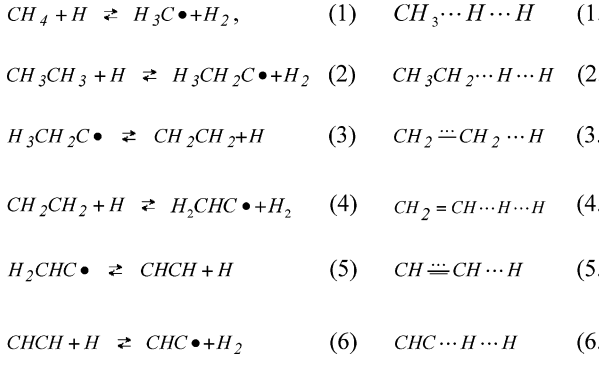

Together with the reaction $CH_3 + CH_3 \rightarrow C_2H_6$, eqs 1−5 produce a viable channel for converting between methane and acetylene. Equation 6 is included to ensure that the conversion stops at C_2H_2 as confirmed in section IV. Equations 1a−6a are the relevant reaction transition states. The combined forward and reverse directions for eqs 1−6 produce a set of 12 elementary reactions that contain a kinetic mechanism for conversion between CH_4 and C_2H_2.

The unimolecular reactions in eqs 1−6 are not influenced by collision if the collision rate constants are much smaller than the reaction rate constants. For the bimolecular reactions, a necessary condition that they are rate-limiting is that the collision rate constant of any related two species is larger than their reaction rate constant. The collision rate constant Z_{AB} between species A and B is given by

$$Z_{AB} = \pi \alpha_{AB} d_{AB}^2 \left(\frac{8kT}{\pi \mu_{AB}}\right)^{1/2} \quad (7)$$

where μ_{AB} is the reduced mass of A and B, α_{AB} is an angular factor with typical values of 0.25−0.30, and d_{AB} is the radius sum of A and B with typical value of 0.1 nm. As shown in Figure 1, the conditions are met under which collision effects do not influence unimolecular and bimolecular reaction rates.

III. Calculations

Ab initio molecular orbital (MO) calculations using the Gaussian94 suite of electronic structure tools[25] were performed to determine input data for the TST rate constants. These data consist of electronic energies, vibration frequencies, and rotational inertia for all species and relevant transition states. These properties of each of the species in our model were previously calculated with ab initio MO methods by many other authors using various levels of theory. Analysis of a system with multiple reaction pathways requires a set of data that has a consistent level of accuracy.

Geometries for all species were optimized at the 6−31g* level using the unrestricted Hartree−Fock approximation for radicals and transition states, and restricted Hartree−Fock calculations for molecules. The transition state option in the code was used to locate reaction transition states, and all transition states were confirmed by frequency analysis to have one imaginary frequency. Zero-point corrections were made for all species. Because only relative reaction rates are of interest in this study, zero-point energy scaling was not carried out, nor was the Wigner−Eckart tunneling correction[26,27] calculated for the barrier height.

The TST rate constant calculation follows the formula $k = (k_B T/h)\exp(-\Delta G^{\circ,\ddagger}/(RT))$,[28] where k_B is Boltzmann constant and $\Delta G^{\circ,\ddagger}$ is the standard activation Gibbs free energy. The unit for k is either $cm^3 \cdot molecule^{-1} \cdot s^{-1}$ for bimolecular reactions or s^{-1} for unimolecular reactions.

The integration of a rate equation is essentially an initial value problem. It can be expressed in matrix form as

$$\frac{d}{dT}\begin{pmatrix} C_{CH_3} \\ C_{CH_4} \\ C_{C_2H_6} \\ C_{C_2H_5} \\ C_{C_2H_4} \\ C_{C_2H_3} \\ C_{C_2H_2} \\ C_{C_2H} \end{pmatrix} = \frac{\mathbf{M}}{T_x v}\begin{pmatrix} C_{CH_3} \\ C_{CH_4} \\ C_{C_2H_6} \\ C_{C_2H_5} \\ C_{C_2H_4} \\ C_{C_2H_3} \\ C_{C_2H_2} \\ C_{C_2H} \end{pmatrix} \tag{8}$$

where **M** is a matrix

$$\begin{pmatrix} -k_{1-}C_{H_2} - k & k_{1+}C_H & 0 & 0 & 0 & 0 & 0 & 0 \\ k_{1-}C_{H_2} & -k_{1+}C_H & 0 & 0 & 0 & 0 & 0 & 0 \\ kC_{CH_3} & 0 & -k_{2+}C_H & k_{2-}C_{H_2} & 0 & 0 & 0 & 0 \\ 0 & 0 & k_{2+}C_H & -k_{2-}C_{H_2} - k_{3+} & k_{3-}C_H & 0 & 0 & 0 \\ 0 & 0 & 0 & k_{+3} & -(k_{3-} + k_{4+})C_H & k_{4-}C_{H_2} & 0 & 0 \\ 0 & 0 & 0 & 0 & k_{4+}C_H & -(k_{4-}C_{H_2} + k_{5+}) & k_{5-}C_H & 0 \\ 0 & 0 & 0 & 0 & 0 & k_{5+} & -(k_{5-} + k_{6+})C_H & k_{6-}C_{H_2} \\ 0 & 0 & 0 & 0 & 0 & 0 & k_{6+}C_H & k_{6-}C_{H_2} \end{pmatrix}$$

and T_x and v are the temperature gradient and the linear flow rate in the chamber axis direction. The quantity k is the rate constant for methyl radical recombination determined experimentally in which a third body collision is included.[29] The quantity $k_{n\pm}$ is the forward (+) or backward (−) rate constant for equation n of $n = 1, ..., 6$. Mathematically eq 8 is a typical stiff equation because β-scission reactions (3+ and 5+) are faster than others by orders of magnitude.[30] The equations are integrated using the fourth order of the Runge−Kutta algorithm.[30] The maximum temperature step is 10^{-8} K for $1900 < T < 2300$ K, and the integration is over the region of 1100−2300 K.

IV. Results

IV.1. Ab Initio Rate Constants. Calculated moments of inertia, electronic energies, and vibration frequencies for all of the species considered are given in Supporting Information Tables IS, IIS, and IIIS, respectively. Arrhenius plots of the TST rate constants using the data in the tables for the six pairs of elementary reactions along with Z_{AB} are shown in Figure 1.

The reaction rates increase with increasing temperature for each of the 12 elementary reactions, and in each case, the bimolecular rate constants are smaller and the unimolecular ones are larger than $Z_{AB}(T)$ under FACVD gas-phase conditions. Therefore, reactions 1−6 are appropriate for determining the reaction kinetics without further consideration of collision effects. From Figure 1, it is clear that the kinetic rate sequence under diamond growth temperatures is

$$\beta\text{-scission} \gg \text{addition} > \text{abstraction} \tag{9}$$

We need to determine how, when taken together, each species controls the system kinetics of the multiple reaction pathways for the conversion between methane and acetylene. This requires that the calculated rate constants reflect the correct relative rate magnitudes among all reaction pathways. To this end, the relations in eq 9 need to be validated by comparison with experimental measurements. Shown in Figures 2 and 3 are Arrhenius plots for reactions 3 and 4 predicted by the present work, along with experimental measurements[31−34] and calculations by Meble et al.[35] Among the experimental measurements for reaction 3, Feng's work[34] is for 400−1000 K and Knyazev's[33] is for 200−3000 K. All measurements together in the range of 1000−2000 K give (3+) > (3−) > (4+) > (4−) in agreement with the present calculations.

Shown in Figure 4 are Arrhenius plots for reactions 5 and 6 predicted by the present work along with experimental measurements.[36] Knyazev et al. suggested that their measurement for reaction 5 is valid over the temperature range 200−2120 K,[36] while Baulch's evaluation of reaction 6 is valid over the

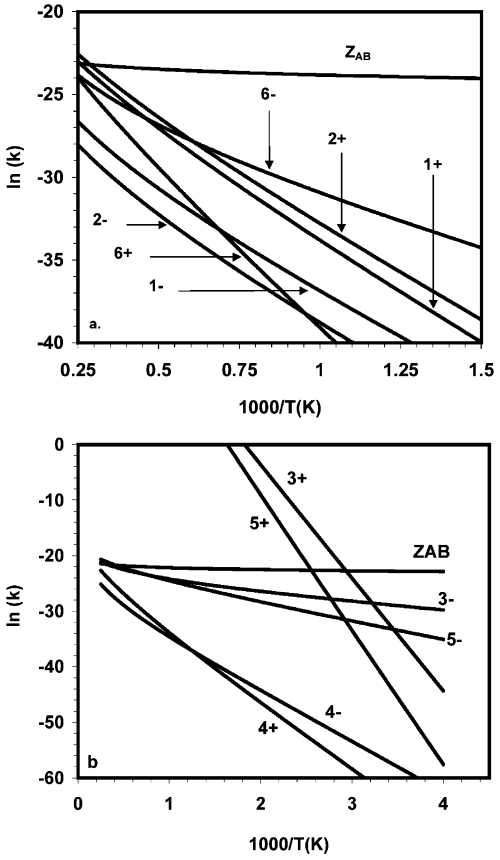

Figure 1. Calculated Arrhenius relations for reactions 1−6. The number *n* corresponds to the reaction in eq *n*. The symbols "+" and "−" refer to the forward and reverse reactions, respectively. Z_{AB} is the collision constant given by eq 7.

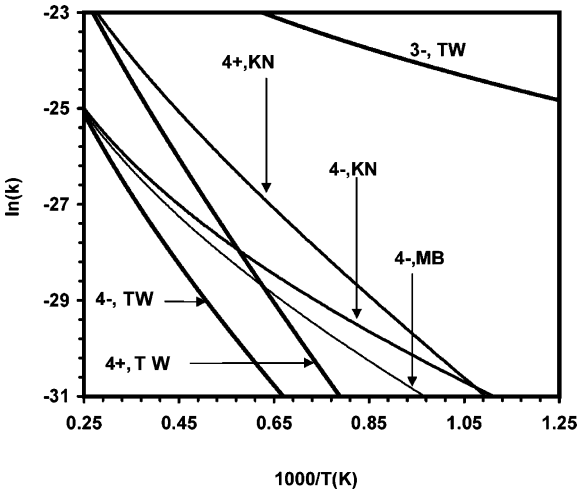

Figure 2. Arrhenius plot comparisons of reactions (4+) and (4−). Calculations include this work (TW) and Mebel et al.[35] (MB). Measurements were made by Knyazev et al.[33] (KN).

temperature range 300−3000 K.[37] Figure 4 illustrates that in the range of temperature 1000−2000 K the referenced rate constants satisfy (5+) > (5−) > (6−) > (6+) in agreement with the present calculations. The relation (6−) > (6+) confirms that the chemical conversion beginning at CH_4 stops at C_2H_2.

Shown in Figure 5 are Arrhenius plots for reactions 1 and 2, along with experimental measurements.[33,38] The measured rate constants follow the sequence (2+) > (1+) >(1−) > (2−) in

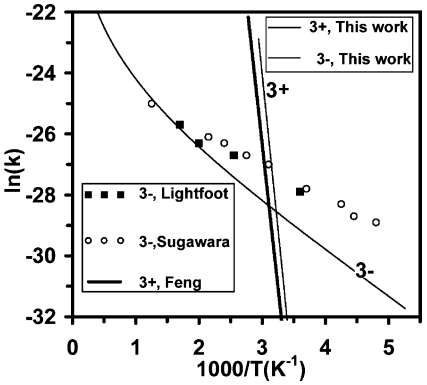

Figure 3. Comparison of Arrhenius relations for the reaction 3 calculated by this work and those measured by Sugawara et al.,[31] Lightfoot et al.,[32] and Feng et al.[34]

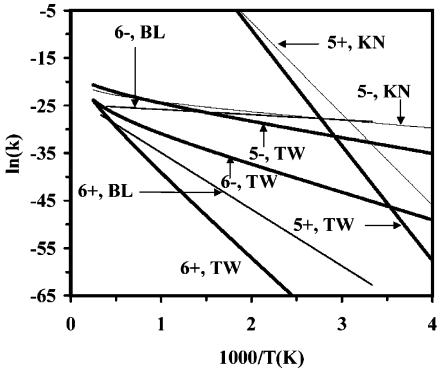

Figure 4. Arrhenius plot comparisons of reactions 5 and 6. Calculations are from this work (TW). Measurements were made by Knyazev et al.[36] (KN). Evaluations were made by Baulch (BL) et al.[37]

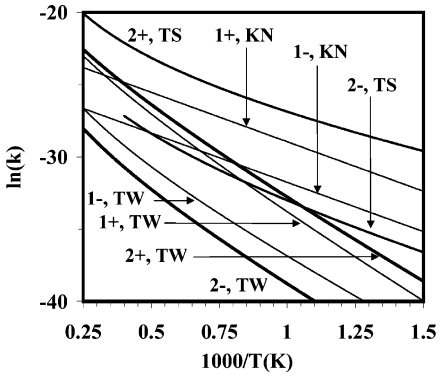

Figure 5. Arrhenius plot comparisons of reactions 1 and 2. Calculated values are from this work (TW). Measurements were made by Knyazev et al.[33] (KN). Evaluations were made by Tsang et al. (TS)[38]

the range of 1000−2000 K as predicted by the present calculation.

The agreement between our calculated values and experimental measurements suggests that our ab initio rate constants possess sufficient accuracy to be a subset of values through which TST can be used to analyze the kinetics of methane conversion to acetylene.

IV.2. Rate Constant Analysis of $CH_4 \rightarrow C_2H_2$. Equation 9 can be used to understand how hydrogen dominates the kinetics of acetylene production through entropy effects. A hydrogen atom that collides with an unsaturated hydrocarbon species has two major reaction pathways. The hydrogen atom may add to the unsaturated carbon−carbon bond, or it may abstract hydrogen to form H_2. While the former is energetically

preferable, the data plotted in Figure 1 suggest that when the temperature is higher than about 500 K, H atom addition to unsaturated carbon species is kinetically unfavorable. This is because at high temperatures, the fast rate for β-scission (which is driven by translational entropy) effectively drives a hydrogen atom back off of the molecule after addition. These two processes of addition and β-scission can continue, leaving the unsaturated molecule susceptible to the slightly less probable abstraction reaction. The radical species after abstraction can lose an additional hydrogen atom via β-scission, a process that can continue until acetylene is formed. Hence, while hydrogen atom addition may be energetically favorable, β-scission reactions maintain unsaturated species in the gas-phase long enough for hydrogen abstraction to drive the system toward acetylene. This system kinetics can be expressed in terms of elementary reactions as

$$CH_2=CH_2+H\begin{cases}\leftrightarrows {}^{\bullet}CH_2-CH_3\\ \rightarrow CH_2CH^{\bullet}+H_2\end{cases} \tag{10}$$

and

$$CH{\equiv}CH+H\begin{cases}\leftrightarrows {}^{\bullet}CH{=}CH_2\\ \leftarrow CH{\equiv}C^{\bullet}+H_2\end{cases} \tag{11}$$

Based on eqs 10 and 11, the following elementary reactions, in agreement with previous model,[11,18,39] can be extracted from eqs 1−6 to explain the conversion of methane to acetylene as observed under typical diamond FACVD conditions[7,40,41]

$$CH_4+H\rightarrow CH_3^{\bullet}+H_2 \tag{12}$$

$$CH_3^{\bullet}+CH_3^{\bullet}+M\rightarrow CH_3CH_3+M^{*} \tag{13}$$

$$CH_3CH_3+H\rightarrow CH_3CH_2^{\bullet}+H_2 \tag{14}$$

$${}^{\bullet}CH_2CH_3\rightarrow CH_2{=}CH_2+H \tag{15}$$

$$CH_2{=}CH_2+H\rightarrow CH_2{=}CH^{\bullet}+H_2 \tag{16}$$

$$CH_2{=}CH^{\bullet}\rightarrow CH{\equiv}CH+H \tag{17}$$

Reaction 13 is a process of radical recombination that is preferable because the energy decrease by C−C bond formation (>80 kcal/mol) is larger than free energy increase, 70 kcal/mol, caused by entropy loss at 1500 K as estimated in section V. In agreement with its experimental rate constant used in our rate equation integration, here a third body is added to ensure bond formation.

The relatively small forward rates for the abstraction reactions 12, 14, and 16 are greatly enhanced by the large rates of the successive reactions eq 13 (radical association) and eqs 15 and 17 (β-scission), as confirmed by our integration of rate equations in section IV.3. Therefore the large rates for these reactions establish the irreversibility of the conversion $CH_4\rightarrow C_2H_2$ at high temperatures, and the overall rate-limiting steps are the abstraction reactions 12, 14, and 16. This relationship between rate-limiting and irreversibility steps had not previously been established.

Equations 12−17 are basically the forward reactions of a generic series of elementary processes suggested before for converting between CH_4 and C_2H_2.[7,8,11,18,39] Our analysis on the system kinetics indicates that the reactions in the backward direction are not kinetically preferable at high temperatures. It is generally believed that the conversion of C_2H_2 to CH_4 must have a mechanism completely different from the reverse pathway of the reactions 12−17.[7,8,18,41]

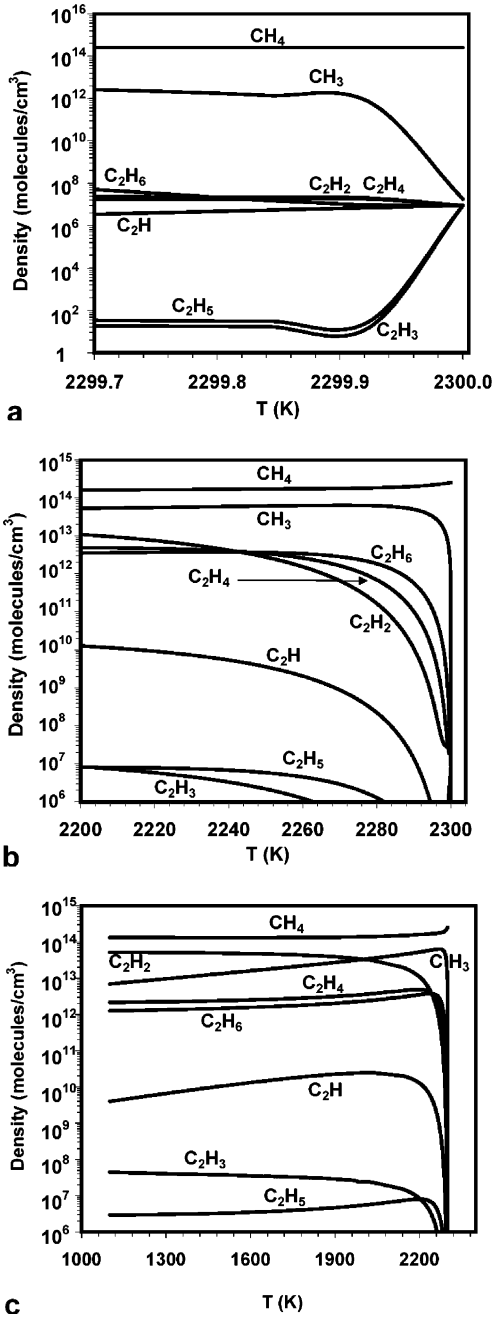

Figure 6. Concentration distributions of carbon-containing species calculated by integration of rate equation: (a) $2299.7 \le T \le 2300.0$ K; (b) $2200 \le T \le 2300$ K; (c) $1100 \le T \le 2300$ K.

IV.3. Integration of Rate Equations. Based on rate constant analysis, we have suggested the chemical kinetics for the conversion of methane to acetylene. Integration of rate eq 8 is needed for additional validation. Plotted in Figure 6 are the results from a first principles kinetics simulation of the gas-phase concentration distribution that clearly demonstrates acetylene production from methane. In this simulation, the filament and substrate temperatures are 2300 and 1100 K, respectively, the total pressure is 20 Torr, the volume flow rate is 100 sccm, and the feed gas composition is 99.7:0.3 for the ratio of H_2/CH_4. Initially, the concentration of CH_3 is 2×10^{-8}, and all other carbon-containing species are 10^{-8} in mole fraction.

We assume that the H atom concentration is linear in the two-dimensional plane of temperature and the logarithmic scale of mole fraction, crossing two points, (1100 K, 2.4×10^{-5}) and (2300 K, 9.9×10^{-3}), based on experimental measurements obtained by third-harmonic generation (THG) and resonance enhanced multiphoton ionization (REMPI).[42−44] The radius for the cross section of the chamber is taken as 8 cm.

The length of the radius, r, is found to be critical in the determination of the temperature range in which acetylene becomes a dominant species. For $r = 0.5$, 0.1 and 0.08 m, the ranges are [2299, 2300], [2190, 2300], and [1990, 2300] respectively. The reason can be attributed to the dependence of v in eq 8, and it is inversely proportional to the radius squared under a given volume flow rate.

The simulation reveals several interesting features of the system. First, there is a sudden change in species concentration when the temperature is near the filament temperature as indicated by Figure 6a. When the feed gas is heated to the chamber temperature, there is a rapid increase in CH_3 concentration due to reaction rates (1+) > (1−). This increase in CH_3 leads to increases in C_2H_6, C_2H_4, C_2H_2 suggesting a conversion from C_1 species to C_2 species. The drop in C_2H_5, C_2H_3, and C_2H can be attributed to the large β-scission rate constants (3+) and (5+), as well as the smaller abstraction rate constant (6−) > (6+). This sudden change is likely not the cause of the ~100 K temperature drop just past the filament that has been measured experimentally in FACVD chambers.[42−46] Instead, the change happens in our calculations because the initial concentration distribution of the feed gas is an artificial mixture and not a natural state for the system. Figure 6a suggests that the system kinetics allows the initial gas mixture to adjust itself quickly to adapt to a new environment. Experimentally, such an adjustment should be finished between the inlet and the filament.

Second, in Figure 6b there is a crossing point (2240 K) at which species contents change from $C_2H_6 > C_2H_4 > C_2H_2$ to $C_2H_6 < C_2H_4 < C_2H_2$ suggesting that there is a fast conversion of CH_4 to C_2H_2. The simulated conversion is due to the forward rate constants of reactions 1−5 being larger than the backward rate constants. Depending on the flow rate, this crossing point can occur at a higher or lower temperature. However, no matter what flow rate is used, this group of rate constants cannot result in reverse conversion.

Third, in the temperature range between 1100 and 2100 K as shown in Figure 6c, the conversion trend continues. The contents for all carbon-containing species follow $CH_4 \approx C_2H_2 > CH_3 > C_2H_4$ in agreement with THG and REMPI measurements.[40,43,47] This sequence is also similar to previous results calculated under local equilibrium conditions.[7,8,11]

Briefly, our simulation reproduces the conversion of CH_4 to C_2H_2. It results from the chemistry predicted in section IV.2 based on rate constant analysis. For a given temperature gradient field and chamber size, all features in Figure 6c will appear in a wider or narrower temperature range depending on the flow rate. This first principles simulation is performed under typical experimental conditions and was found to reproduce experimental measurements, supporting the idea that the FACVD gas-phase chemistry can be effectively explored via analysis of rate constants.

Similar kinetic concentration distributions were also obtained in previous work using fluid mechanics.[14,15,21,22,48] Our elementary reaction sets are smaller than those previously employed. A small number of elementary reactions is essential for us to decompose the complex kinetics into single species properties.

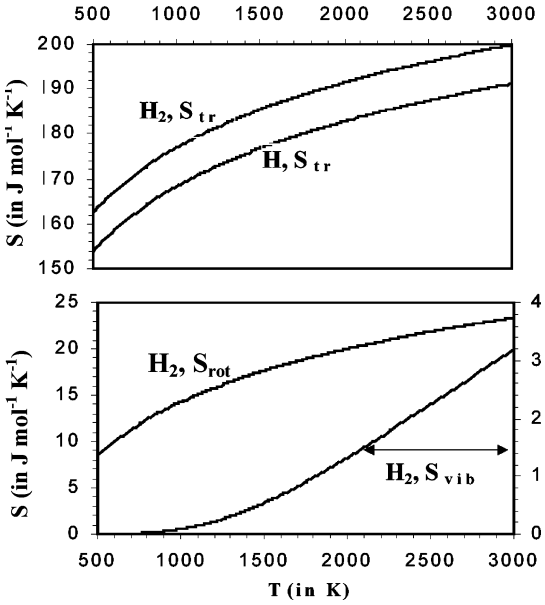

Figure 7. Order of magnitude comparison of the contributions of translational, rotational, and vibrational entropy to the total entropy for a hydrogen atom and molecule.

V. Discussion

The two approaches in sections IV.2 and IV.3 were used to demonstrate that under conditions typical of FACVD (i.e., 1100−2300 K[42−44]), the formation of acetylene from methane is kinetically favored via reactions 12−17 and the backward reaction of eq 6. Such conversion kinetics is essentially dominated by hydrogen via entropy, as shown below.

V.1. Entropy Contributions. In TST, rate constants can be expressed as

$$k_c = \left(\frac{k_B T}{h}\right)\exp\left(\frac{\Delta S_c^{\circ,\ddagger}}{R}\right)\exp\left(-\frac{\Delta H_c^{\circ,\ddagger}}{RT}\right) \qquad (18)$$

where the total change in entropy is a sum of the changes in translational, rotational, vibrational, and electronic entropy changes:

$$\Delta S_c^{\circ,\ddagger} = \Delta S_{c,tr}^{\circ,\ddagger} + \Delta S_{c,rot}^{\circ,\ddagger} + \Delta S_{c,vib}^{\circ,\ddagger} + \Delta S_{c,el}^{\circ,\ddagger} \qquad (19)$$

While all terms are included in our calculations, a qualitative analysis of their contribution is necessary to understand the system kinetics. To this end, some approximations are required.

The electronic entropy is $R\ln 2$ for radicals and zero for other species. $\Delta S_{c,el}^{\circ,\ddagger} = 0$ because of total spin conservation. The contribution from the other three terms is illustrated in Figure 7 for H and H_2, where the absolute entropy arising from translation, rotation, and vibration are plotted. From the figure, it is clear that for H_2

$$S_{tr} \gg S_{rot} \gg S_{vib}$$

or specifically

$$S_{tr}/S_{rot} \approx 10, \quad \text{for} \quad T < 2000 \text{ K}$$

$$S_{rot}/S_{vib} \approx 10, \quad \text{for} \quad 800 \text{ K} < T < 1500 \text{ K} \qquad (20)$$

and that the translational entropy of H and H_2 are of the same order of magnitude.

Relation 20 implies that under conditions for diamond film growth, the most significant contribution to the entropy comes

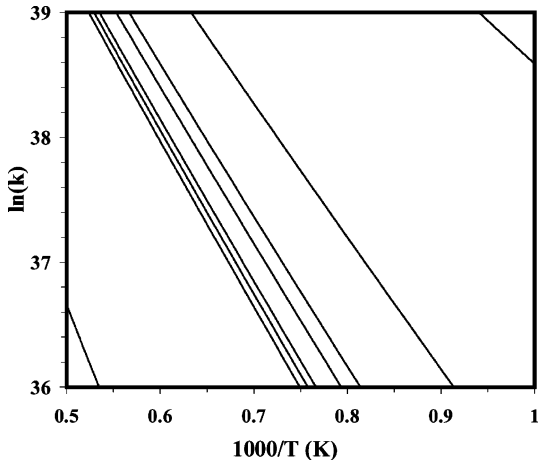

Figure 8. Arrhenius plots of the abstraction reactions neglecting entropy. The eight curves in the figure are (6+), (4+), (2−), (1+), (1−), (2+), (4−), and (6−) from left to right.

from changes in the number of translational degrees of freedom or, equivalently, species creation or annihilation. For example, creation of an H atom will increase entropy by over 150 J/(mol K). A 2-fold increase in mass, such as occurs when H is converted to H_2 via abstraction, only results in an additional $R\ln(2)^{3/2} = 8.6$ J/K to the translational entropy. When the number of species is conserved for a given reaction, changes in rotational entropy are the next largest effect. In the abstraction reactions 1, 2, 4, and 6, there is no net change in the number of species; therefore, changes in translational entropy do not greatly influence reaction rates in either direction. However, there is a net annihilation of rotational entropy in the reverse reaction due to the loss of H_2.

From Figure 7, it can be concluded that vibrational entropy can also be largely ignored. The vibrational entropy is a summation over $3n - 6$ terms, each of which is a function of one vibrational frequency. For two nonlinear species containing n_1 and n_2 atoms to form a transition state of $n_1 + n_2$ atoms, the net decrease in the number of vibrational frequencies (not counting the imaginary frequency associated with the transition state coordinate) is $[(3n_1 - 6) + (3n_2 - 6)] - [3(n_1 + n_2) - 6] - 1 = 5 =$ constant. From Figure 7, it is clear that the typical ratio of rotational to vibrational entropy of one frequency is ~10 at 1500 K; therefore, ignoring vibrational entropy is reasonable if there is a change in rotational entropy.

V.2. Entropy Limitations on Abstraction Reactions. Our calculations and analysis show that the favorable directions of abstraction reactions 1, 4, and 6 can be explained by entropy effects and that the preferred direction of reaction 2 is a result of reaction enthalpy. Reactions 1, 4, and 6 exhibit crossing points as a function of temperature between the forward and reverse directions.

From Figure 1, the forward reactions of 1 and 4 are favored because the gas-phase temperature is higher than that at the crossing point. If there were no contributions from entropy to the rate constants, the Arrhenius plots for the four reactions would be those plotted in Figure 8. There are no crossing points between the forward and reverse reactions, and in each case, the reverse reaction is preferred over the corresponding forward reaction. When translational entropy is added into the rate constants, the reverse reactions are still preferable, although the difference between the reverse and forward reactions is reduced slightly. This can be explained from the data in Table 1. The data show that the state R−H + H is more stable than R* + H_2. Therefore with their common transition state, $\Delta H_+^{\circ,\ddagger} > \Delta H_-^{\circ,\ddagger}$. However, the translational entropy of H_2 is larger than that of H, $|\Delta S_+^{\circ,\ddagger}| < |\Delta S_-^{\circ,\ddagger}|$, where both $\Delta S_+^{\circ,\ddagger}$ and $\Delta S_-^{\circ,\ddagger}$ are negative. Therefore the difference between $\Delta G_+^{\circ,\ddagger}$ and $\Delta G_-^{\circ,\ddagger}$ or k_+ and k_- is reduced by translational entropy. If rotational entropy is further taken into account k_- is lowered only at high temperatures relative to k_+, leading to the crossing points. Because H has no rotational degree of freedom, k_+ is relatively unchanged. The forward direction of reactions 1 and 4 can be attributed to the creation of the H_2 rotational free degree.

TABLE 1: Molar Formation Enthalpy (MFE, kJ/mol) for Reactions 1−6 in the Forward Direction[a]

reactions	MFE
$CH_4 + H \rightarrow H_3C^{\bullet} + H_2$	3.590
$CH_3CH_3 + H \rightarrow H_3CH_2C^{\bullet} + H_2$	−7.360
$H_3CH_2C^{\bullet} \rightarrow CH_2CH_2 + H$	153.9
$CH_2CH_2 + H \rightarrow H_2CHC^{\bullet} + H_2$	19.33
$H_2CHC^{\bullet} \rightarrow CHCH + H$	170.6
$CHCH + H \rightarrow CHC^{\bullet} + H_2$	92.65

[a] Only electronic energy and zero point energy are accounted for. Other terms that contribute to enthalpy are canceled by the corresponding terms in entropy during calculation of Gibbs free energy.

From Figure 8 and the data in Table 1, it is clear that the enthalpy difference between the species on either side of eq 6 is much larger than the other abstraction reactions. Because of this, entropy effects remain smaller than enthalpy contributions to the rate constants, and the reverse reaction of eq 6 is preferred. As mentioned above, this causes the reaction sequence to terminate at acetylene formation.

For reaction 2, $k_+ > k$, both in Figure 1 and Figure 8. From Table 1, $\Delta H_+^{\circ,\ddagger} < \Delta H_-^{\circ,\ddagger}$, which accounts for $k_+ > k_-$ in Figure 8. Based on the foregoing discussion on entropy effects, the difference between (2+) and (2−) is further increased by translational entropy, and k_- is further lowered by rotational entropy. Therefore the forward direction for reaction 2 is favored over all temperatures.

V.3. Entropy Limitations on Addition Reactions. The remaining two reactions, 3 and 5, are affected much more by entropy. Addition of an H atom to unsaturated carbon is energetically downhill with a reaction energy barrier no higher than 10 kcal/mol. The reverse process, β-scission, has a reaction barrier ~30 kcal/mol higher than that of addition. However, as discussed above, the increase in the number of translational degrees of freedom associated with β-scission drives eqs 3 and 5 in the forward direction at high temperatures. From Figure 1b, our calculations predict that β-scission is kinetically favored over hydrogen addition beginning at 400 K, 173 K lower than that observed by Rye.[49] As the temperature goes up over 1000 K, Figures 2 and 4 illustrate that β-scission is about $e^{20} \approx 10^{17}$ times faster than addition. This result suggests that the addition of hydrogen atoms to unsaturated carbon is entropy-limited in the gas phase for diamond film growth.

The conclusion of entropy-limited H addition agrees with Frenklach's observation, based on numerical simulation, that H addition is at least not a dominant chemical path to suppress π-bond formation.[14] The concept of entropy-limited addition is also consistent with two experimental measurements.[49,50] Balooch and Olander generated atomic hydrogen of partial pressure 1.5 Torr by thermal dissociation of H_2 in an effusion oven at $T = 2500$ K.[50] Modulated molecular beam mass spectrometric measurements showed that acetylene is the only carbon-containing product from the pyrolytic reaction of hydrogen atoms with graphite when $T_{graphite} > 1000$ K. This result indicates that H does not chemically add to acetylene at high

temperature. Rye generated H using a hot tungsten filament and showed by mass spectrometry that unsaturated carbon containing species can be saturated to CH_4 by H addition only when $T_{graphite} < 573$ K.[49]

Entropy-limited hydrogen addition can be extended to the general case of uniradical addition to carbon π-bonds in the gas phase. In general, hydrogen addition represents the most favorable case for addition reactions of single σ-bond formation. To form a transition state, hydrogen addition loses the smallest amount of entropy because hydrogen has the lightest weight and no rotational degrees of freedom. The H atom has the least steric hindrance, and its 1s orbital has a tendency to form almost the strongest covalent bond with carbon (next to C−F σ-bond only), leading to almost the largest amount of enthalpy decrease. Therefore, among all possible addition reactions in FACVD, hydrogen has the lowest Gibbs barrier. Because our calculations predict that hydrogen addition is unfavorable, it can be concluded that addition of any other uniradical to an unsaturated carbon under the gas-phase conditions typical of diamond growth is also unfavorable. Using a molecular mechanics approach, Harris and Belton[51] calculated the addition of acetylene to surface radicals during diamond growth and suggested that the addition reaction is not preferable due to loss of translational entropy. This is an example of entropy-limited uniradical addition to a carbon π-bond. Application of the concept of entropy-limited uniradical addition may significantly simplify chemical analysis of similar gas-phase environments, such as those in combustion and other CVD.

VI. Summary

The kinetics of converting methane to acetylene under low pressure and high-temperature conditions was analyzed with ab initio TST rate constants and rate equation integration, assuming a set of six reactions and 12 rates (one rate for the forward and backward directions of each reaction). Using completely ab initio data produces rates with a consistent level of accuracy, while TST allows entropic and enthalpic contributions as a function of temperature to be explicitly analyzed. For the acetylene production, our calculations suggest a chemical and physical mechanism of how hydrogen dominates the kinetics through entropy effects at the molecular level. Specifically, we show that β-scission reactions, the rates for which are greatly enhanced by translational entropy at high temperatures, restrict the addition of hydrogen (and other radical species) to unsaturated carbon−carbon bonds. This yields a relatively high concentration of unsaturated carbon species that can undergo hydrogen abstraction. Rotational entropy determines the direction of the rate-limiting abstraction reactions. The net effect of abstraction and β-scission reactions is to drive the system irreversibly to acetylene. Non-hydrogen radical addition to carbon π-bond creates a weaker σ-bond and loses more entropy than that of hydrogen. We therefore suggested that non-hydrogen radical addition to carbon π-bond is entropy forbidden under FACVD conditions.

Acknowledgment. Y.L. and D.W.B. are supported by the National Science Foundation and the Office of Naval Research. X.D. and C.S. were supported by the National Key Laboratory of Theoretical and Computational Chemistry at Jilin University. We appreciate Dr. Clifford Padgett for critically proof reading this manuscript.

Supporting Information Available: Listed in Tables IS, IIS, and IIIS are calculated moments of inertia, vibrational frequencies, and electronic energies for all of the species including transition states. This material is available free of charge via the Internet at http://pubs.acs.org.

References and Notes

(1) Zhao, Y.; Truhlar, D. G. *J. Phys. Chem. A* **2005**, *109*, 5656.
(2) Li, Y. X.; Brenner, D. W. *Phys. Rev. Lett.* **2004**, *92*, No. 075503.
(3) Angus, J. C.; Hayman, C. C. *Science* **1988**, *241*, 913.
(4) Garrison, B. J.; Dawnkaski, E. J.; Srivastava, D.; Brenner, D. W. *Science* **1992**, *255*, 835.
(5) Butler, J. E.; Geis, M. W.; Krohn, K. E.; Lawless, J., Jr.; Deneault, S.; Lyszczarz, T. M.; Flechtner, D.; Wright, R. *Semicond. Sci. Technol.* **2003**, *18*, S67.
(6) Nesladek, M. *Semicond. Sci. Technol.* **2005**, *20*, R19.
(7) Goodwin, D. G.; Butler, J. E. *Theory of Diamond Chemical Vapor Deposition*; Dekker: New York, 1997.
(8) Ashfold, M. N. R.; May, P. W.; Petherbridge, J. R.; Rosser, K. N.; Smith, J. A.; Mankelevich, Y. A.; Suetin, N. V. *Phys. Chem. Chem. Phys.* **2001**, *3*, 3471.
(9) Sommer, M.; Mui, K.; Smith, F. W. *Solid State Commun.* **1989**, *69*, 775.
(10) Piekarczyk, W.; Roy, R.; Messier, R. *J. Cryst. Growth.* **1989**, *98*, 765.
(11) Li, Y. X.; Brenner, D. W.; Dong, X. L.; Sun, C. C. *Mol. Simul.* **2000**, *25*, 41.
(12) Dandy, D. S. *Thin Solid Films* **2001**, *381*, 1.
(13) Haubner, R. *Diamond Relat. Mater.* **2004**, *13*, 648.
(14) Frenklach, M. *J. Appl. Phys.* **1989**, *65*, 5142.
(15) Harris, S. J. *J. Appl. Phys.* **1989**, *65*, 3044.
(16) Frenklach, M.; Wang, H. *Phys. Rev. B* **1991**, *43*, 1520.
(17) Molinari, E.; Polini, R.; Sessa, V.; Terranova, M. L.; Tomellini, M. *J. Mater. Res.* **1993**, *8*, 785.
(18) Mankelevich, Y. A.; Suetin, N. V.; Ashfold, M. N. R.; Smith, J. A. et. al. *Diamond Relat. Mater.* **2001**, *10*, 364.
(19) Goodwin, D. G. *Appl. Phys. Lett.* **1991**, *59*, 277.
(20) Coltrin, M. E.; Dandy, D. S. *J. Appl Phys* **1993**, *74*, 5803.
(21) Dandy, D. S.; Coltrin, M. E. *J. Appl Phys* **1994**, *76*, 3102.
(22) Ruf, B.; Behrendt, F.; Deutschmann, O.; Warnatz, J. *J. Appl. Phys.* **1996**, *79*, 7256.
(23) Truhlar, D. G.; Garrett, B. C.; Klippenstein, S. J. *J. Phys. Chem.* **1996**, *100*, 12771.
(24) Frenklach, M. Theory and Models for Nucleation and Growth of Diamond Films. In *Diamond and Diamond-Like Films and Coatings*; Clausing, R. E., et al., Eds.; NATO-ASI Series B, Physics, Vol. 266; Plenum Press: New York, 1991.
(25) Frisch, M. J.; Trucks, G. W.; Schlegel, H. B.; Gill, P. M. W.; Johnson, B. G.; Robb, M. A.; Cheeseman, J. R.; Keith, T.; Petersson, G. A.; Montgomery, J. A.; Raghavachari, K.; Al-Laham, M. A.; Zakrzewski, V. G.; Ortiz, J. V.; Foresman, J. B.; Cioslowski, J.; Stefanov, B. B.; Nanayakkara, A.; Challacombe, M.; Peng, C. Y.; Ayala, P. Y.; Chen, W.; Wong, M. W.; Andres, J. L.; Replogle, E. S.; Gomperts, R.; Martin, R. L.; Fox, D. J.; Binkley, J. S.; Defrees, D. J.; Baker, J.; Stewart, J. P.; Head-Gordon, M.; Gonzalez, C.; Pople, J. A. *Gaussian 94*, revision B.2; Gaussian, Inc.: Pittsburgh, PA, 1995.
(26) Hase, W. L.; Schlegel, H. B.; Balbyshev, V.; Page, M. *J. Phys. Chem.* **1996**, *100*, 5354.
(27) Eckart, C. *Phys. Rev.* **1930**, *35*, 1303.
(28) Moore, J. W.; Pearson, R. G. *Kinetics and Mechanism*; John Wiley & Sons: New York, 1981.
(29) Wang, B.; Hou, H.; Yoder, L. M.; Muckerman, J. T.; Fockenberg, C. *J. Phys. Chem. A* **2003**, *107*, 11414.
(30) Steinfeld, J. I.; Francisco, J. S.; Hase, W. L. *Chemical Kinetics and Dynamics*; Prentice Hall: Upper Saddle River, NJ, 1999.
(31) Sugawara, K. I.; Okazaki, K.; Sato, S. *Bull. Chem. Soc. Jpn.* **1981**, *54*, 2872.
(32) Lightfoot, P. D.; Pilling, M. J. *J. Phys. Chem.* **1987**, *91*, 3373.
(33) Knyazev, V. D.; Bencsura, A.; Stoliarov, S. I.; Slagle, I. R. *J. Phys. Chem.* **1996**, *100*, 11346.
(34) Feng, Y.; Niiranen, J. T.; Bencsura, A.; Knyazev, V. D.; Gutman, D.; Tsang, W. *J. Phys. Chem.* **1993**, *97*, 871.
(35) Mebel, A. M.; Morokuma, K.; Lin, M. C. *J. Chem. Phys.* **1995**, *103*, 3440.
(36) Knyazev, V. D.; Slagle, I. R. *J. Phys. Chem.* **1996**, *100*, 16899.
(37) Baulch, D. L.; Cobos, C. J.; Cox, R. A.; Esser, C.; Frank, P.; Just, T.; Kerr, J. A.; Pilling, M. J.; Troe, J.; Walker, R. W.; Warnatz, J. *J. Phys. Chem. Ref. Data* **1992**, *21*, 411.
(38) Tsang, W.; Hampson, R. F. *J. Phys. Chem. Ref. Data* **1986**, *15*, 1087.
(39) Dong, X. L.; Li, Y. X.; Sun, C. C. *Chin. J. Comput. Phys.* **1996**, *13*, 439.
(40) Celii, F. G.; Pehrsson, P. E.; Wang, H. T.; Butler, J. E. *Appl. Phys. Lett.* **1988**, *52*, 2043.
(41) Butler, J. E.; Woodin, R. L. *Philos. Trans. R. Soc. London, Ser. A* **1993**, *342*, 209.

(42) Connell, L. L.; Fleming, J. W.; Chu, H. N.; Vestyck, D. J., Jr.; Jensen, E.; Butler, J. E. *J. Appl. Phys.* **1995**, *78*, 3622.
(43) Zumbach, V.; Schafer, J.; Tobai, J.; Ridder, M.; Dreier, T.; Schaich, T.; Wolfrum, J.; Ruf, B.; Behrendt, F.; Deutschman, O.; Warnatz, J. *J. Chem. Phys.* **1997**, *107*, 5918.
(44) Redman, S. A.; Chung, C.; Rosser, K. N.; Ashfold, M. N. R. *Phys. Chem. Chem. Phys.* **1999**, *1*, 1415.
(45) Chen, K.-H.; Chuang, M.-C.; Penney, C. M.; Banholzer, W. F. *J. Appl. Phys.* **1992**, *71*, 1485.
(46) Menningen, K. L.; Childs, M. A.; Anderson, L. W.; Lawler, J. E. *Rev. Sci. Instrum.* **1996**, *67*, 1546.
(47) Smith, J. A.; Cameron, E.; Ashfoid, M. N. R.; Mankelevich, Y. A.; Suetin, N. V. *Diamond Relat. Mater.* **2001**, *10*, 358.
(48) Goodwin, D. G.; Gavillet, G. G. *J. Appl. Phys.* **1990**, *68*, 6393.
(49) Rye, R. R. *Surf. Sci.* **1977**, *69*, 653.
(50) Balooch, M.; Olander, D. R. *J. Chem. Phys.* **1975**, *63*, 4772.
(51) Harris, S. J.; Belton, D. N. *Jpn. J. Appl. Phys.* **1991**, *30*, 2615.